INTERNATIONAL JOURNAL FOR NUMERICAL METHODS IN FLUIDS
Int. J. Numer. Meth. Fluids 2008; **56**:1061–1067
Published online 20 September 2007 in Wiley InterScience (www.interscience.wiley.com). DOI: 10.1002/fld.1606

Reduced modelling of blood flow in the cerebral circulation: Coupling 1-D, 0-D and cerebral auto-regulation models

J. Alastruey[1, 2, *, †], S. M. Moore[3], K. H. Parker[2], T. David[3], J. Peiró[1] and S. J. Sherwin[1]

[1]*Department of Aeronautics, South Kensington Campus, Imperial College London, London SW7 2AZ, U.K.*
[2]*Department of Bioengineering, South Kensington Campus, Imperial College London, London SW7 2AZ, U.K.*
[3]*Centre for Bioengineering, University of Canterbury, Private Bag 4800, Christchurch, New Zealand*

SUMMARY

Pulsatile blood flow in the cerebral circulation is simulated using a nonlinear, one-dimensional model of the arterial haemodynamics coupled in the time domain with lumped parameter and flow auto-regulation models of the perfusion of the microcirculation. A linear analysis of the coupling shows that a resistance equal to the characteristic impedance of the blood vessel is required at the inflow of a terminal windkessel model to avoid the generation of non-physiological wave reflections. The cerebral model suggests that the worst anatomical variation of the circle of Willis in terms of restoring normal cerebral flows after a sudden carotid occlusion is a circle without the first segment of the contralateral anterior cerebral artery.

Received 29 March 2007; Revised 23 July 2007; Accepted 23 July 2007

KEY WORDS: 1-D flow modelling; lumped parameter models; cerebral auto-regulation; circle of Willis

1. INTRODUCTION

A good understanding of pulse wave propagation in the normal cardiovascular system and the impact of disease and anatomical variations on the propagation patterns provide valuable information for clinical diagnosis and treatment. One-dimensional (1-D) modelling efficiently simulates the problem because of the large pulse wavelengths compared with arterial diameters. While three-dimensional (3-D) models are typically limited to local areas of the system because of their computational cost, 1-D models offer a good compromise between accuracy and cost when a

*Correspondence to: J. Alastruey, Department of Aeronautics, South Kensington Campus, Imperial College London, London SW7 2AZ, U.K.
†E-mail: jordi.alastruey-arimon@imperial.ac.uk

Contract/grant sponsor: EPSRC Advanced Research Fellowship

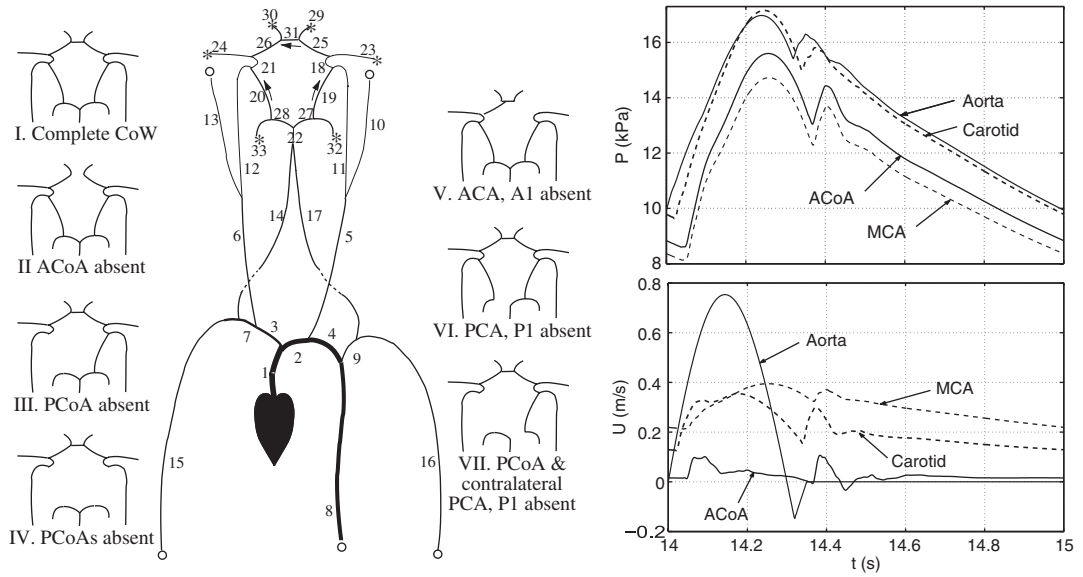

Figure 1. Schematic representation of the 1-D arterial network used to simulate cerebral blood flow and the anatomical variations studied. The following arteries are included: aorta (1,2,4,8), brachiocephalic (3), subclavians (7,9), brachials (15,16), carotids (5,6,10,11,12,13,18,21), vertebrals (14,17), basilar (22), PCoAs (19,20), ACoA (31), MCAs (23,24), ACAs (25,26,29,30), and PCAs (27,28,32,33). Terminal branches coupled with RCR windkessel models (○) or 0-D cerebral auto-regulation models (∗). The panels show pressure and velocity waveforms in ascending aorta (1), right common carotid (6), right MCA (24), and ACoA (31).

more general simulation is required. However, the large number of vessels in the full arterial and venous systems (the number increases exponentially as more generations of bifurcations are introduced) makes it impossible to model all vessels using the 1-D formulation. Consequently, even the 1-D model has to be truncated after few generations of bifurcations. The haemodynamic effect of vessels beyond the 1-D model arteries can be accounted for using lumped parameter or zero-dimensional (0-D) models relating the flow to pressure.

This investigation focuses on the coupling of the nonlinear, time-domain, 1-D formulation with 0-D models. It addresses some numerical and physical issues of the coupling. In particular, we show how cerebral flow auto-regulation can be simulated using a lumped parameter model. These algorithms are then applied to assess the effects on cerebral flows of a sudden carotid occlusion, taking into account the most frequent anatomical variations of the circle of Willis (CoW) and using the 1-D arterial network from our previous work in [1] (Figure 1).

2. PROBLEM FORMULATION

2.1. The 1-D model

Conservation of mass and momentum applied to a 1-D impermeable and deformable tubular control volume of incompressible and Newtonian fluid provides the hyperbolic system of partial

DOI: 10.1002/fld

differential equations (PDEs)

$$\begin{aligned} \frac{\partial A}{\partial t} + \frac{\partial (AU)}{\partial x} &= 0 \\ \frac{\partial U}{\partial t} + U\frac{\partial U}{\partial x} + \frac{1}{\rho}\frac{\partial P}{\partial x} &= \frac{f}{\rho A} \end{aligned} \tag{1}$$

where x is the axial coordinate along the vessel, t is the time, $A(x,t)$ is the cross-sectional area of the vessel, $U(x,t)$ is the average axial velocity, $P(x,t)$ is the average internal pressure over the cross section, ρ is the density of the blood, and $f = -2\mu\pi(\alpha/(\alpha-1))U$ is the friction force per unit length, in which μ is the blood viscosity and α is a non-dimensional correction factor that depends on the assumed velocity profile. The system of governing equations can be completed with the tube law

$$P = \frac{\beta}{A_0}(\sqrt{A} - \sqrt{A_0}), \quad \beta(x) = \frac{4}{3}\sqrt{\pi}hE \tag{2}$$

which assumes a thin, homogeneous, incompressible and elastic arterial wall with a thickness $h(x)$, a Young's modulus $E(x)$, and a sectional area $A_0(x)$ at the reference state $(P,U) = (0,0)$.

Riemann's method of characteristics applied to Equations (1) and (2) shows that changes in pressure and velocity are propagated forward by W_f at a speed of $U + c$ and backward by W_b at a speed of $U - c$. If β and A_0 are constant along x and $f = 0$, $W_{\mathrm{f,b}} = U \pm 4(c - c_0)$, $c(A) = \sqrt{(\beta/2\rho A_0)}A^{1/4}$, and $c_0 = c(A_0)$.

The 1-D equations are solved in arterial networks using a discontinuous Galerkin scheme with a Legendre polynomial spectral/*hp* spatial discretization and a second-order Adams–Bashforth time-integration scheme. This algorithm, which has been successfully tested against *in vitro* data [2], involves the solution of Riemann problems at the interfaces of each artery, at the junctions and at the inflow and outflow boundaries. Further details on the 1-D model are given in [3].

2.2. 0-D models and their coupling with 1-D models

The coupling between a 1-D domain and a 0-D model is established through the solution of a Riemann problem at their interface (Figure 2, left). An intermediate state (A^*, U^*) originates at time $t + \Delta t$ (Δt is the time step) from $(A_\mathrm{L}, U_\mathrm{L})$ and $(A_\mathrm{R}, U_\mathrm{R})$ at time t. The state $(A_\mathrm{L}, U_\mathrm{L})$ corresponds to the end point of the 1-D domain, and $(A_\mathrm{R}, U_\mathrm{R})$ is a virtual state selected so that (A^*, U^*) satisfies the relation between A^* and U^* dictated by the 0-D model used. According to the method of characteristics,

$$W_\mathrm{f}(A^*, U^*) = W_\mathrm{f}(A_\mathrm{L}, U_\mathrm{L}) \tag{3}$$

$$W_\mathrm{b}(A^*, U^*) = W_\mathrm{b}(A_\mathrm{R}, U_\mathrm{R}) \tag{4}$$

since $U \ll c$ under physiological conditions. A mathematical analysis of this coupling is given in [4]. The 1-D boundary condition is imposed by assuming $A_\mathrm{R} = A_\mathrm{L}$ to close the problem, which leads to

$$U_\mathrm{R} = 2U^* - U_\mathrm{L} \tag{5}$$

DOI: 10.1002/fld

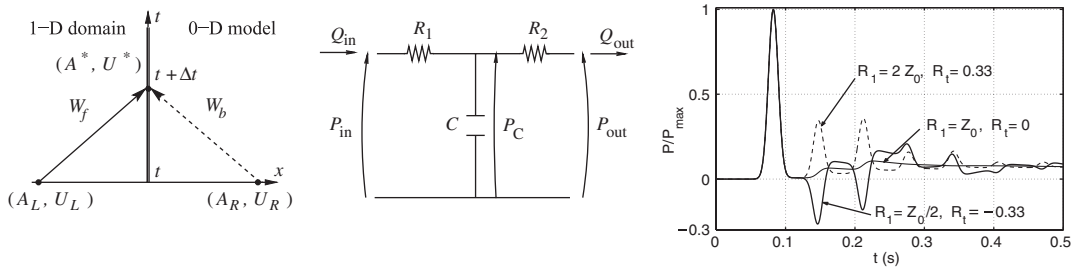

Figure 2. (Left) Notation for the Riemann problem. (Middle) RCR windkessel model depicted using the electric analogy. (Right) Effect of R_1 on the propagation of a Gaussian wave in a single 1-D domain coupled to an RCR model.

2.2.1. Terminal resistance (R) model. This model simulates the peripheral circulation as a purely resistive load R, in which the state (A^*, U^*) satisfies $A^*U^* = (P(A^*) - P_{\text{out}})/R$, where P_{out} is the venous pressure assumed to be constant. Combined with Equations (2) and (3) yields a nonlinear equation in A^*

$$\mathscr{F}(A^*) = R[U_{\text{L}} + 4c(A_{\text{L}})]A^* - 4Rc(A^*)A^* - \frac{\beta}{A_0}(\sqrt{A^*} - \sqrt{A_0}) + P_{\text{out}} = 0 \tag{6}$$

that is solved using Newton's method with the initial guess $A^* = A_{\text{L}}$. Once A^* has been obtained, U^* is calculated as $U^* = (P(A^*) - P_{\text{out}})/A^*R$ and the boundary condition is prescribed through Equation (5).

Linearization of Equations (1) and (2) yields $\tilde{W}_{\text{b}} = -R_{\text{t}}\tilde{W}_{\text{f}} - 2P_{\text{out}}/A_0/(R + Z_0)$, where $\tilde{W}_{\text{f,b}} = U^* \pm (c_0/A_0)A^*$ are the linear Riemann invariants [3], $R_{\text{t}} = (R - Z_0)/(R + Z_0)$ is the terminal reflection coefficient and $Z_0 = \rho c_0/A_0$ is the characteristic impedance of the 1-D vessel. Note that when R tends to infinity, R_{t} tends to 1 (full reflection), and when $R = 0$, $R_{\text{t}} = -1$ (open end). The terminal resistance model completely absorbs any incoming wave when $R = Z_0$ so that $R_{\text{t}} = 0$.

2.2.2. Matched three-element (RCR) windkessel model. This model accounts for the resistance, R, and the compliance, C, of the peripheral vessels using the RCR windkessel model shown in Figure 2 (middle). According to Section 2.2.1, we consider $R_1 = Z_0$ to let any incoming wave reach the CR_2 system without being reflected. Waves are reflected by the CR_2 system, which is governed by

$$C\frac{\mathrm{d}P_C}{\mathrm{d}t} = A^*U^* - \frac{P_C - P_{\text{out}}}{R_2} \tag{7}$$

where P_C is the pressure at C and $R_2 = R - R_1$. The coupling is solved as for the R model (Section 2.2.1), but with $P_{\text{out}} = P_C$ and $R = R_1$. At every time step n, P_C is determined by solving a first-order time discretization of Equation (7), $P_C^n = P_C^{n-1} + \Delta t/C(A_{\text{L}}U_{\text{L}} - (P_C^{n-1} - P_{\text{out}})/R_2)$, with $P_C^{n-1} = 0$ for $n = 1$.

DOI: 10.1002/fld

2.3. The cerebral auto-regulation model

The brain is particularly dependent on the cerebral circulation since it has a high metabolic rate and is very sensitive to ischaemia (insufficient blood supply). Sufficient blood supply to the brain is maintained by a network of collateral vessels, the CoW being the main collateral pathway, and a precise system of auto-regulation by vasodilatation and vasoconstriction that can alter each cerebral resistance R. We assume that the concentration of CO_2 in the brain tissue (C_tCO_2) is the driving force for changes in R. The CO_2 produced by brain metabolism diffuses into the blood stream and is removed by the cerebral blood flow (CBF) per unit mass of brain tissue perfused. For a constant cerebral metabolism, if CBF is reduced, C_tCO_2 increases and the pH in the tissue decreases [5], producing smooth muscle relaxation [6] and, hence, reducing R. The change in C_tCO_2 is simulated as the difference between the rate of production of CO_2 in the tissue (equal to the rate of consumption of O_2, $CMRO_2$, which is assumed to be 0.035 ml O_2/g brain/min) and the rate of removal of CO_2 by the CBF,

$$\frac{dC_tCO_2}{dt} = CMRO_2 - CBF(t)(C_tCO_2 - C_aCO_2) \tag{8}$$

where C_aCO_2 is the concentration of CO_2 in arterial blood, which is governed by pulmonary circulation and is assumed to be constant in this study, $C_aCO_2 = 0.5$ ml CO_2/g brain. Any further chemical reactions are implicitly incorporated into the dynamic for R, which is postulated to be a function of C_tCO_2,

$$\frac{dA_R}{dt} = G_R(C_tCO_{2SP} - C_tCO_2) \tag{9}$$

where A_R represents an auto-regulation activation for R to change, $G_R = 20$ is a proportional gain to match the transient dynamics measured in [7], and C_tCO_{2SP} is the normal or set point C_tCO_2, which is given as the steady-state solution of Equation (8), $C_tCO_{2SP} = C_aCO_2 + CMRO_2/CBF_{SP}$, where CBF_{SP} is the set point CBF. R is obtained from the sigmoidal function

$$R = \frac{R_L + R_U e^{A_R - \hat{C}}}{1 + e^{A_R - \hat{C}}} \tag{10}$$

where R_U and R_L are the upper and lower limits of $R(t)$ during auto-regulation, respectively, and $\hat{C} = -\log[(R_{SP} - R_L)/(R_U - R_{SP})]$ is a constant to ensure that for $A_R = 0$, $R = R_{SP}$. We consider $R_L = 0.74R_{SP}$ based on the experimental data for the normotensive group in [8]. R_U is assumed to be $1.30R_{SP}$.

This auto-regulation model is coupled to a terminal resistance model (Section 2.2.1) at the outlet of each cerebral artery in Figure 1. In each iteration, Equations (8) and (9) are solved for C_tCO_2 and A_R using a fourth-order Runge–Kutta scheme, with CBF calculated from the flow at the outlet of the 1-D domain, A_LU_L, assuming a total brain mass of 1.5 kg distributed among the cerebral arteries in the same proportion as the flow distribution determined by R_{SP}. Once A_R is known, $R(t)$ is determined using Equation (10), Equation (6) is solved for A^* and the boundary condition is prescribed through Equation (5).

DOI: 10.1002/fld

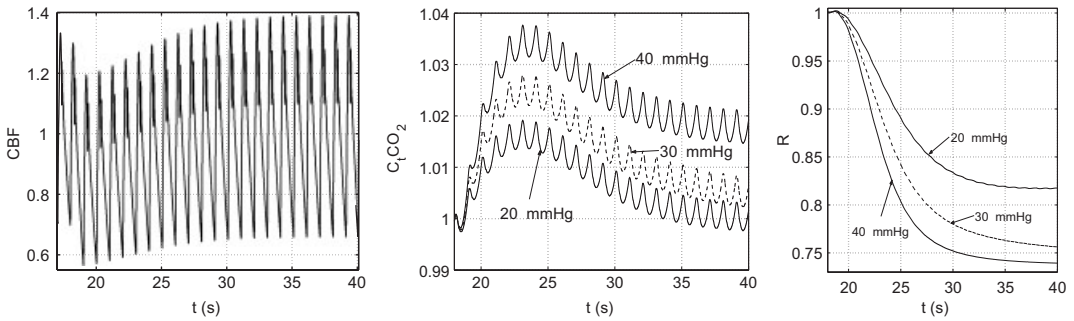

Figure 3. CBF (left), C_tCO_2 (middle) and R (right) time histories in the right MCA (vessel 24 in Figure 1) after introducing pressure drops of 20 (only case shown for CBF), 30 and 40 mmHg in the right carotid artery (vessel 6). Variables are non-dimensionalized by their corresponding set point values.

3. RESULTS AND DISCUSSION

Figure 2 (right) shows the effect of coupling an RCR model with $R_1 \neq Z_0$ to a single 1-D domain in which a Gaussian wave is propagated. Unless $R_1 = Z_0$, significant reflected waves are generated by the RCR model, since $R_t \neq 0$ in R_1 according to Section 2.2.1. If $R_1 = Z_0$, waves are only reflected by the CR_2 system, and the RCR model produces more physiological waveforms in an arterial network as the system shown in Figure 1. This figure shows pressure and velocity waveforms simulated using the arterial network in [1], with the inflow velocity at the ascending aorta shown in the figure. R_{SP} in the six cerebral arteries are set to the values that yield the set point flows reported in [9] for normal subjects. This model is used to study the effects on cerebral flows of reductions in their afferent blood pressures caused by sudden obstructions in the flow, particularly during surgical procedures such as carotid endarterectomy (surgical incision to remove plaque in patients with a severe stenosis), angioplasty (balloon expansion) and stenting (introduction of a mesh to keep the lumen open after angioplasty).

Figure 3 shows the CBF, C_tCO_2 and R time histories in the right middle cerebral artery (MCA) for different pressure drops in the middle of the right carotid artery. The sudden decrease in CBF caused by the pressure drop yields an increase in C_tCO_2, according to Equation (8), which produces a decrease in R through Equations (9) and (10). This mechanism restores CBF_{SP} in all the cerebral arteries of the complete CoW for pressure drops of up to 30 mmHg (Table I). For a pressure drop of 40 mmHg, R reaches its lower limit of $0.74R_{SP}$ and CBF_{SP} and C_tCO_{2SP} cannot be fully restored (Figure 3). However, the expected increase in the O_2 extraction [10] might ensure sufficient O_2 delivery. The flows in the right posterior cerebral artery (PCA) and all left cerebral arteries are less affected by the right carotid occlusion, since they are perfused by the basilar and left carotid arteries.

Among the anatomical variations considered (see Figure 1), the absence of the first segment of the left anterior cerebral artery (ACA), (case V) is the worst scenario in terms of the amount of CBF_{SP} restored by the auto-regulation model, particularly in the right MCA and ACA and the left ACA. Furthermore, our results show that the anterior communicating artery (ACoA) is a critical collateral pathway to compensate for carotid occlusions, particularly in the right MCA and ACA (Table I). These two findings are in agreement with [1], in which only the compensatory ability of the CoW itself was assessed, without accounting for vasodilatation and vasoconstriction.

DOI: 10.1002/fld

Table I. Percentage of CBF_{SP} restored after auto-regulation in the right ACA, MCA, and PCA (vessels 30, 24 and 33 in Figure 1) for different pressure drops (20–30–40 mmHg) in the right carotid (vessel 6).

	Complete CoW	Anatomical variation II	Anatomical variation V
Anterior cerebral artery (ACA)	100–100–97	100–92–82	100–91–81
Middle cerebral artery (MCA)	100–99–92	100–93–82	100–92–82
Posterior cerebral artery (PCA)	100–100–100	100–100–100	100–100–100

4. CONCLUSIONS

Pulse wave propagation in the cerebral circulation has been simulated using a multiscale approach involving a 1-D model for the main cerebral arteries and a 0-D model for the control of the terminal resistances. The complex chemical pathways of cerebral auto-regulation have been simplified by assuming that CO_2 is the driving force for vasodilatation and vasoconstriction. We have used variables with a direct physiological meaning and parameters that can be obtained from human experimental data. This model allows us to better understand the factors that increase the risk of cerebral ischaemia during surgical procedures in the afferent arteries of the CoW, and highlights the potential of reduced modelling to provide clinically valuable and fast information when applied to patient-specific data.

REFERENCES

1. Alastruey J, Parker KH, Peiró J, Byrd SM, Sherwin SJ. Modelling the circle of Willis to assess the effects of anatomical variations and occlusions on cerebral flows. *Journal of Biomechanics* 2007; **30**:1794–1805.
2. Matthys KS, Alastruey J, Peiró J, Khir AW, Segers P, Verdonck PR, Parker KH, Sherwin SJ. Pulse wave propagation in a model human arterial network: ASSESSMENT of 1-D numerical simulations against *in vitro* measurements. *Journal of Biomechanics* 2007; DOI: 10.1016/j.jbiomech.2007.05.027.
3. Sherwin SJ, Franke V, Peiró J, Parker KH. One-dimensional modelling of a vascular network in space–time variables. *Journal of Engineering Mathematics* 2003; **47**:217–250.
4. Fernández MA, Milišić V, Quarteroni A. Analysis of a geometrical multiscale blood flow model based on the coupling of ODEs and hyperbolic PDEs. *SIAM Multiscale Modelling and Simulation* 2005; **4**:215–236.
5. Cady EB, Chu A, Costello AMD, Delpy DT, Gardiner RM, Hope PL, Reynolds EOR. Brain intracellular pH and metabolism during hypercapnia and hypocapnia in the new-born lamp. *Journal of Physiology* 1987; **382**:1–14.
6. Tian R, Vogel P, Lassen NA, Mulvany MJ, Andreasen F, Aalkjaer C. Role of extracellular and intracellular acidosis for hypercapnia-induced inhibition of tension of isolated rat cerebral arteries. *Circulation Research* 1995; **76**(2):269–275.
7. Newell DW, Aaslid R, Lam A, Mayberg TS, Winn HR. Comparison of flow and velocity during dynamic autoregulation testing in humans. *Stroke* 1994; **25**(4):793–797.
8. Strandgaard S. Autoregulation of cerebral blood flow in hypertensive patients. The modifying influence of prolonged antihypertensive treatment on the tolerance to acute, drug-induced hypotension. *Circulation* 1976; **53**(4):720–727.
9. Fahrig R, Nikolov H, Fox AJ, Holdsworth DW. A three-dimensional cerebrovascular flow phantom. *Medical Physics* 1999; **26**(8):1589–1599.
10. Derdeyn CP, Videen TO, Yundt KD, Fritsch SM, Carpenter DA, Grubb RL, Powers WJ. Variability of cerebral blood volume and oxygen extraction: stages of cerebral haemodynamics impairment revisited. *Brain* 2002; **125**:595–607.